NANO LETTERS

pubs.acs.org/NanoLett Letter

Green Fluorescent Carbon Dots with Critically Controlled Surface States: Make Silk Shine via Feeding Silkworms

Zhao-Fan Wu, Bao-Juan Wang, Jia-Wen Ni, Zhao-Nan Sun, Xi-Rong Zhang, and Huan-Ming Xiong*

Cite This: *Nano Lett.* 2024, 24, 9675−9682 Read Online

ACCESS | Metrics & More | Article Recommendations | Supporting Information

ABSTRACT: Feeding silkworms with functional materials as additives to produce naturally modified silk is a facile, diverse, controllable, and environmentally friendly method with a low cost of time and investment. Among various additives, carbon dots (CDs) show unique advantages due to their excellent biocompatibility and fluorescence stability. Here, a new type of green fluorescent carbon dots (G-CDs) is synthesized with a high oil−water partition ratio of 147, a low isoelectric point of 5.16, an absolute quantum yield of 71%, and critically controlled surface states. After feeding with G-CDs, the silkworms weave light yellow cocoons whose green fluorescence is visible to the naked eye under UV light. The luminous silk is sewn onto the cloth to create striking patterns with beautiful fluorescence. Such G-CDs have no adverse effect on the survival rate and the life cycle of silkworms and enable their whole bodies to glow under UV light. Based on the strong fluorescence, chemical stability, and biological safety, G-CDs are found in the digestive tracts, silk glands, feces, cocoons, and even moth bodies. G-CDs accumulate in the posterior silk glands where fibroin protein is secreted, indicating its stronger combination with fibroin than sericin, which meets the requirements for practical applications.

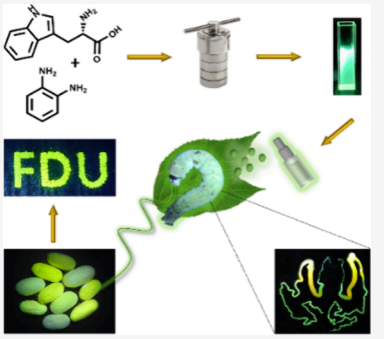

KEYWORDS: *Biosafety, Carbon dots, Feeding silkworms, Fluorescence, Lipophilicity*

For thousands of years, silkworms have been fed by humans to produce silk for various textiles.[1] After modification by modern science and technology, the application of silk has been expanded to drug delivery, tissue engineering, biological imaging, and so on.[2−6] The modification methods mainly include changing silk surfaces by chemical reagents, recombining the DNA of silkworms by genetic engineering, and feeding silkworms by functional substances.[7−9] The postmodification processes have been industrialized which often cause environmental pollution, and the chemicals usually damage the internal structure of silk protein. The genetic modification requires a long time of research and a huge economic cost, and the successful products are rare at present.[10,11] In contrast, adding functional substances to feed silkworms is easy to design and simple to operate, which can endow silk with various modifications in a short time.[12,13] So far, various substances have been developed and fed to silkworms. For example, single-walled carbon nanotubes (SWNTs) and graphene were fed to silkworms to gain mechanically enhanced silk.[14] The feed of Ag nanowire (Ag NW) modified diets improves not only the mechanical properties but also electrical and thermal conductivities,[15] and the rare earth ions, metal nanoparticles, polymer dots, organic dye, and AIE molecules were employed as feed additives to obtain silk with enhanced mechanical and antibacterial properties, UV resistance, different colors and fluorescence, respectively.[16−21]

Among the reported additives, carbon dots (CDs), a new type of zero-dimensional carbon nanoparticles with excellent optical properties and good biocompatibility, have shown unique advantages beyond their counterparts.[22,23] The synthetic routes of CDs include "top-down" and "bottom-up" approaches, and the latter has been adopted more frequently in recent years.[24−26] The precursors for CDs include various biomass, small molecules, macromolecules, and polymers.[27−29] In the family of fluorescent materials, CDs have better photostability and chemical stability than organic dyes and possess lower biotoxicity and easier degradation than metal-based quantum dots/metal oxide nanoparticles.[30−32] Moreover, the structure of precursors, reactant ratio, solvent, temperature, and time can be finely adjusted to regulate the fluorescence emission wavelength, quantum yield, particle size, and surface functional groups of CDs.[33−35] Although CDs are commonly used in LED lighting, biosensing, imaging, and fluorescence analyses, their tunable fluorescence properties and low toxicity make it possible to produce on a large scale for feeding silkworms to obtain fluorescent silk.[36−40] So far, there are only several reports on raising silkworms with CDs. In 2019, blue fluorescent CDs were fed to silkworm to obtain modified silk with increased mechanical properties and intrinsic fluorescence, but the fluorescence of such silk could only be seen under a laser

Received: May 23, 2024
Revised: July 20, 2024
Accepted: July 22, 2024
Published: July 26, 2024

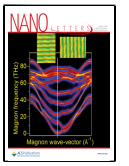

https://doi.org/10.1021/acs.nanolett.4c02426
Nano Lett. 2024, 24, 9675−9682

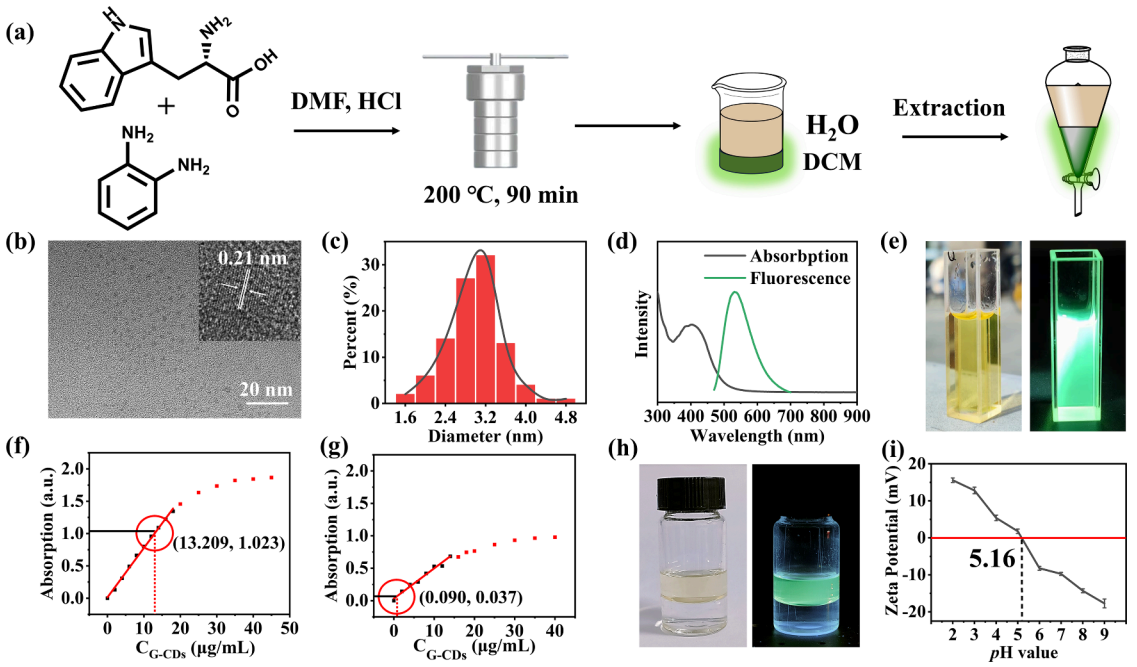

Figure 1. (a) Schematic path of G-CDs preparation. (b) TEM and the inset HRTEM images of G-CDs. (c) Diameter distribution of G-CDs. (d) UV−vis absorption and PL emission curves of G-CDs (excitation wavelength = 450 nm). (e) Photos of G-CD ethanol solutions in (left) daylight and (right) UV light, respectively. (f) Photos under an incandescent and UV lamp for the distribution of G-CDs (6 $\mu g \cdot mL^{-1}$) in the mixture (volume ratio of *n*-octanol/PBS = 1). The concentration standard curves of UV−vis absorption of G-CDs are (g) $y = 0.0764x + 0.0138$ in *n*-octanol, $R^2 = 0.9961$, $c = 13.209\ \mu g \cdot mL^{-1}$ and (h) $y = 0.0466x + 0.0328$ in phosphate buffer saline (PBS), $R^2 = 0.9839$, $c = 0.090\ \mu g \cdot mL^{-1}$, respectively. Calculation of the oil/water partition coefficient: Lg $P = 13.209/0.090 = 2.167$. (i) Zeta potentials of G-CDs in aqueous solutions with different pH values.

confocal microscope.[41] In 2022, red fluorescent silk visible to the naked eye was produced successfully by feeding silkworms with the mulberry leave derived carbon dots (R-CDs) with deep red fluorescence, but such R-CDs were found more in the sericin and would be removed after degumming.[42] Therefore, it is a great challenge to produce fluorescent silk fabrics based on CDs with other colors in which CDs are located mainly in the fibroin.

In the present work, two small molecules with conjugation planes and high lipophilicity are selected as precursors to prepare CDs together because some highly lipophilic and weakly acidic substances are apt to enter the posterior silk gland where fibroin protein is secreted.[43,44] After careful adjustment and optimization, the as-prepared G-CDs showed strong emission at 535 nm with a high quantum yield of 71%. Their oil−water partition concentration ratio is up to 147 times (Lg $P > 2$), and their isoelectric point is 5.16, which is close to that of the posterior silk gland. The G-CD-fed silkworms emitted strong green fluorescence in their bodies and produced brightly green fluorescent cocoons, both of which were visible to the naked eye under UV light. The control experiments proved that G-CDs had no influence on the silkworm life cycle and did not transfer to the silkworm eggs, which means the next generation of the tested silkworms is not influenced either. G-CDs were mainly found in the posterior silk gland of silkworms, which proved that G-CDs were apt to combine with the fibroin. The optical features of G-CDs remained in the silk glands, feces, and cocoons, demonstrating their excellent fluorescence stability, chemical stability, and biological safety. Finally, the obtained fluorescent cocoons were reeled to threads and sewn on the cloth to show striking patterns, indicating that the natural fluorescent fibers could be used on a large scale.

Figure 1 displays the preparation route of G-CDs, in which *o*-phenylenediamine (*o*-PDA) and L-tryptophan (L-Try) are selected as the synthetic precursors. They were dissolved in DMF containing a few catalytic HCl and then heated at 200 °C for 90 min in a Teflon-lined autoclave. After cooling to room temperature, the reaction solution was poured into water followed by extraction by dichloromethane (DCM). The product was extracted repeatedly in a separatory funnel until the water phase was colorless. The oil phase (DCM solution) was collected and dried naturally to obtain G-CDs. Figure 1 b is the transmission electron microscope (TEM) image of G-CDs with the inset high-resolution TEM (HRTEM) image, in which the nanoparticles are uniform and monodispersed, with the lattice spacing of 0.21 nm, corresponding to the (100) crystal face of graphitic carbon, which may derive from the structures formed at the initial stages of bottom-up synthesis.[45−47] Figure 1 c presents the particle size distribution of G-CDs counted by TEM in which the average diameter of G-CDs is about 3 nm. The TEM results are in accord with the detailed investigation by HRTEM shown in Figure S1. Figure 1 d shows the UV−visible absorption spectra and photoluminescence (PL) spectra of G-CD ethanol solutions, confirming that the sample has a typical n−π^* transition of aromatic sp^2 structure[38,48] and strong green emission at 535 nm. Figure 1 e illustrates the sample's photos in sunlight and UV light, respectively, indicating that G-CDs have very strong fluorescence efficiency. The absolute quantum yield (QY) of our G-CDs measured by an integrating sphere is 71%, much higher than many other green emissive CDs in the literature.

It should be noted that although *o*-PDA and L-Try can produce CDs at the same solvothermal conditions our G-CDs are a new kind of CDs. The *o*-PDA-derived CDs show yellow emission at 575 nm (Figure S2 a), while the L-Try-derived CDs exhibit blue emission at 467 nm (Figure S2 b). When the G-CD solution is excited by different wavelengths of light from 420 to

https://doi.org/10.1021/acs.nanolett.4c02426
Nano Lett. 2024, 24, 9675−9682

470 nm, the emission peaks locate at about 540 nm constantly (Figure S2 c), which proves that G-CDs are not a simple mixture of the above two kinds of CDs. In addition, G-CDs are very stable under continuous irradiation of 450 nm (Figure S3), which proves their good resistance to photobleaching. The oil/water partition coefficient (Lg P) is commonly used to quantify lipophilicity in the biomedical fields, and here *n*-octanol and PBS solution are chosen as the solvents. The shake flask method is employed to test the Lg P of G-CDs.[49−52] Figure 1 f shows that only the upper *n*-octanol layer is luminescent under UV light, verifying G-CDs are lipophilic. According to the absorbance values of the upper and lower layers as well as standard curves, the retention concentrations of G-CDs in the two layers after sufficient distribution are calculated to be 13.209 and 0.090 $\mu g \cdot mL^{-1}$, respectively (Figure 1 g and h). That is, the concentration ratio in the oil/water phase is about 147, and the corresponding Lg P is 2.167, suggesting that G-CDs have excellent lipophilicity. It was reported that when Lg $P > 2$ feed additives can migrate to the silk glands through the digestive tract of silkworms.[18,53] Besides, the lower isoelectric point (pI, the pH value when Zeta potential is zero) of the additive materials favors their enrichment in the silk glands of silkworms.[53,54] In Figure 1 i, the pI value of G-CDs is estimated by measuring the Zeta potential at different pH values, and the result of 5.16 indicates that G-CDs are weakly acidic.[20,21,55] Therefore, both high lipophilicity and weak acidity of G-CDs favor their transportation in silkworm bodies to silk glands.

Figure 2 reveals the internal chemical structure of the G-CDs. In the IR spectra (Figure 2 a), the 3500−3000 cm^{-1} broad band

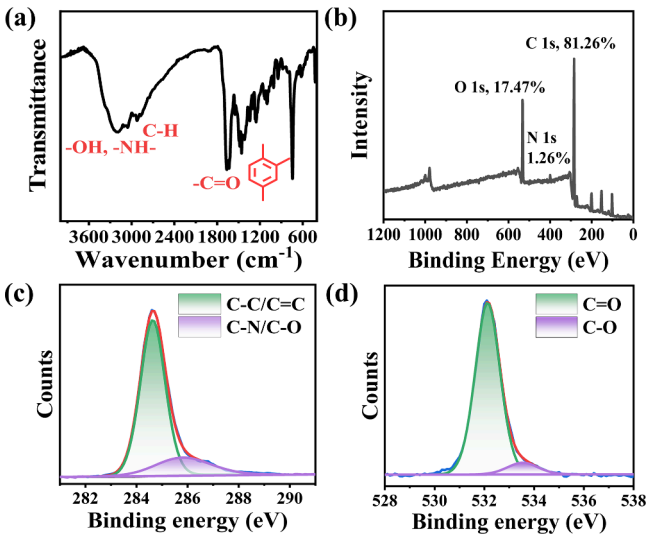

Figure 2. (a) FT-IR spectra of G-CDs. (b) Full scan XPS data of G-CDs. The peak fitting analyses of the fine XPS (c) C 1s and (d) O 1s for G-CDs.

is attributed to the stretching vibration of −OH and −NH−, and the sharp peak at 1680 cm^{-1} is assigned to the stretching vibration of −C═O, confirming the existence of a carboxyl group and the secondary amine, respectively.[37] The band of 3136−3000 cm^{-1} and the strong peak at 742 cm^{-1} are separately ascribed to the stretching vibration and out-of-plane bending vibration of C−H on the aromatic ring, as well as the band of 1620−1450 cm^{-1} derived from the stretching vibration of the benzene ring.[56,57] The band of 2853−2923 cm^{-1} originates from the stretching vibration of C−H on the saturated carbon. The full scan X-ray photoelectron spectroscopy (XPS) in Figure 2 b presents the element composition of the G-CDs. The C 1s fine spectrum in Figure 2 c can be divided into two peaks: C−C/C═C (284.6 eV) and C−N/C−O (285.8 eV), respectively. G-CDs have low N content, and the fine N 1s spectrum is divided into two peaks of C═N (399.0 eV) and C−N (400.1 eV) (Figure S4). The O 1s fine spectrum can be separated into the peaks of C═O (532.1 eV) and C−O (533.5 eV) (Figure 2 d).[58,59] In addition, the XRD spectrum of G-CDs (Figure S5) displays a broad peak at about 25°, confirming the (002) lattice of the graphite structure.[60] In the Raman spectra (Figure S6), the intensity ratio of the D-band (disordered carbon, 1343 cm^{-1}) and G-band (graphitic carbon, 1597 cm^{-1}) is 1.04, indicating the interlaced structure of graphite and defect carbon in G-CDs.[61] The Raman peak at 1450 cm^{-1} may be derived from the N-doping effect, suggesting the existence of five- or seven-membered rings.[46,62]

Figure 3 portrays the luminescent phenomena of living silkworms, as well as their cocoons, moths, and eggs. Silkworms feed on mulberry leaves. Their whole lives are divided into five ages, and the fifth age is the mature silkworm stage, which lasts for 7−9 days, when the amount of mulberry leaves is the largest, the body weight increases quickly, and the silk gland develops rapidly. From the third day of the fifth instar, the G-CD ethanol solutions were sprayed on the mulberry leaves and dried to feed the experimental silkworms, while the control group was fed as before.[21] After 2 days of feeding, the luminescence of silkworms could be seen clearly by the naked eye and investigated by a stereofluorescence microscope. In Figure 3 a, the whole body of an experimental silkworm shows intense green fluorescence, including its head, chest, and tail (Figure 3 b ∼ d). In contrast, the control silkworm only shows fluorescence in its head (Figure 3 e ∼ g), which is ascribed to its autofluorescence.[63] Under the UV lamp, the control silkworm shows no fluorescence (Figure 3 h), which agrees well with Figure 3 f and g. The body weights of all silkworms at the fifth instar increase synchronously, and the final weights of the experimental groups are slightly higher than those of the control (Figure 3 i). Figure S7 manifests the whole process of the experimental silkworms from egg to maturity, cocoon, copulation, laying eggs, and hatching of the second-generation eggs, certifying no impact of G-CDs on the lifecycle of silkworms. Moreover, all groups survived and wove cocoons successfully with almost zero mortality.

By the end of the fifth instar, a moving silkworm (Movie 1) and a cocooning silkworm (Movie 2) in the experimental group were filmed under UV light. In Movie 1, the fluorescence is observed mainly in the large blood vessels and every joint on the back of the silkworm, indicating that G-CDs are enriched in these parts. In Movie 2, the silkworm is spinning bright silk, which verifies that G-CDs are transferred from its body to the cocoon. Figure 3 j is a screenshot from Movie 2. A lot of cocoons are produced in this way (Figure S8). Under white light, the control cocoons are light brown or pale pink (Figure 3 k), while the experimental cocoons look light yellow (Figure 3 m). Under UV light, the control cocoons appear dim with faint colors (Figure 3 l), while experimental cocoons exhibit bright green fluorescence (Figure 3 n). Figure 3 o and Figures S9 and S10 exhibit that the experimental female moths have green fluorescence on their abdomen, whereas no fluorescence was observed in the control moths. All of the moths were able to mate and lay eggs normally, and the fresh eggs show light yellow color under daylight and faint yellow fluorescence under UV light, with no significant difference between the control and the

https://doi.org/10.1021/acs.nanolett.4c02426
Nano Lett. 2024, 24, 9675−9682

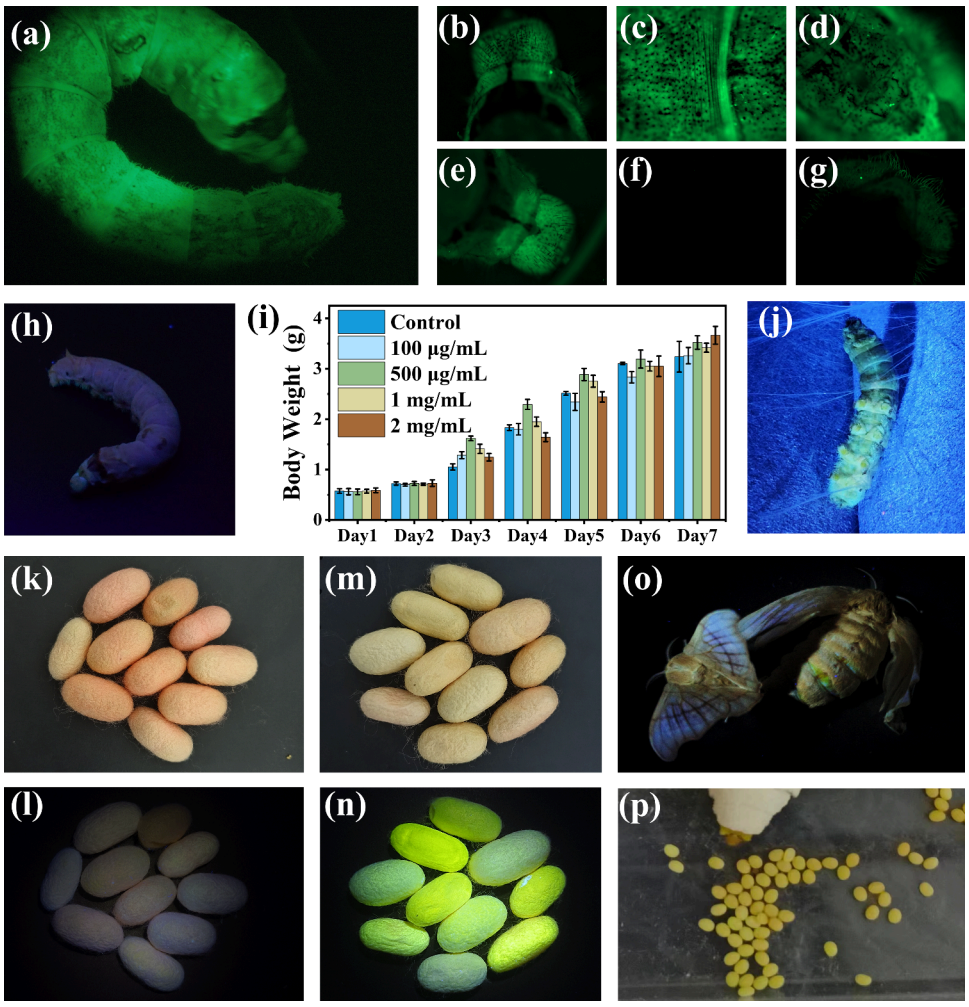

Figure 3. (a) Experimental silkworm under a stereofluorescence microscope. After eating G-CDs, the silkworm's fluorescence images of the (b) head, (c) chest and abdomen, and (d) tail. (e) For the control group under the same microscope, only the head is fluorescent, while the (f) chest and abdomen and (g) tail have almost no fluorescence. (h) A silkworm of the control group under a UV lamp. (i) The body weight variation during the fifth instar of the experimental silkworms that have eaten different concentrations of G-CDs, compared with the control. (j) An experimental silkworm is weaving a cocoon under UV light. (k) The cocoons of the control group under white and (l) UV light and those of the experimental group under (m) white and (n) UV light, respectively. (o) The mating silkworm moths of the experimental group under UV light. (p) The fresh eggs laid by the above silkworm moths under white light.

experimental groups. These results suggest that G-CDs are not transmitted to the next generation of experimental silkworms, avoiding the potential influence of G-CDs on the offspring.

Figure 4 provides detailed analyses of the morphology, fluorescence, and composition of the obtained silk and meanwhile explores the application of this novel luminescent fiber in silk woven artware. The loose silk was collected from the outer layer of the dry cocoons and compared in Figure 4 a. The control silk appears light pink in daylight and shows no fluorescence under UV light, while the experimental silk looks pale yellow in daylight and shines bright green under UV irradiation. These two kinds of silk were extracted with ethanol, and the obtained solutions are shown in Figure 4 b. Both of them are yellow in daylight, due to the pigments from mulberry leaves.[64,65] Under UV light, the control extract has a weak blue fluorescence, while the experimental one emits strong green fluorescence. Their PL spectra in Figure 4 c verify the difference in both luminescence color and intensity between two samples, and the experimental one has a PL peak at 535 nm which is coincident with G-CDs. Both the TEM and HRTEM images in Figure 4 d also agree with those of G-CDs (Figure 1 b). These results testify that G-CDs are indeed present in the cocoons and silk of the experiment group and responsible for the typical green luminescence. SEM images of the two silk samples do not show any difference (Figure 4 e and f), which means that the incorporation of G-CDs does not destroy the natural silk morphology. The experimental cocoon silk was reeled to one spool (Figure 4 g ∼ h), which also shows green fluorescence under UV light. The patterns of "FDU" were sewn on the red and the black cloth with the fluorescent silk, respectively (Figure 4 i ∼ l), which emit beautiful and striking green fluorescence under UV light. Since such fluorescent silk has eminent toughness to support the requirement of decoration and embroidery, the G-CDs incorporation can endow high value to the natural silk.

Figure 5 shows the distribution and metabolic pathways of G-CDs in the silkworm body. At the end of the fifth instar of silkworm, the intake of mulberry is enough, and a large amount of sericin and fibroin protein is synthesized in the silk gland. After the residual mulberry leaves and water are excreted out through feces and urine, the silkworm begins to spin, when the gelatinous substance in the silk gland is transformed into silk

https://doi.org/10.1021/acs.nanolett.4c02426
Nano Lett. 2024, 24, 9675−9682

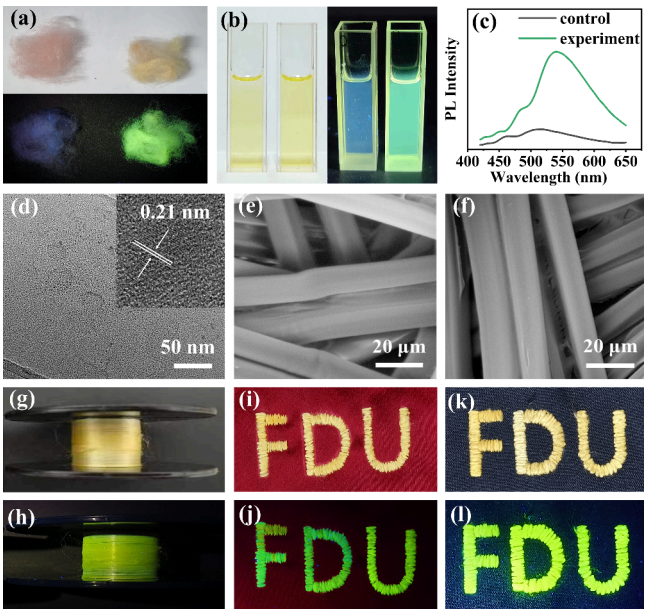

Figure 4. (a) Loose silk from (left) the control and (right) the experimental groups under (upper) white and (bottom) UV light, respectively. (b) The ethanol solutions extracted from the two samples of (a) under (left) white and (right) UV light, respectively. (c) PL emission spectra of the two samples of (b). (d) TEM image of the ethanol extract from the cocoon of the experimental group, with the inset HRTEM image. (e) SEM images of the cocoon of the control and (f) the experimental group. (g) A spool with silk reeled from the cocoons of the experimental group under white and (h) UV light, respectively. FDU patterns embroidered on red cloth under (i) white and (j) UV light and on black cloth under (k) white and (l) UV light, respectively.

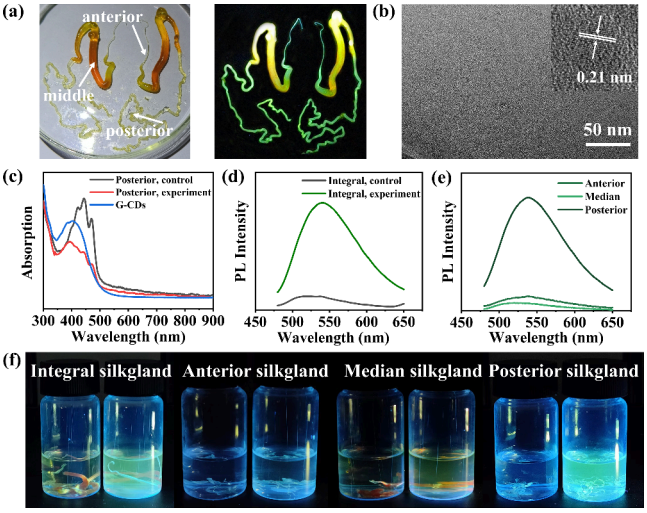

Figure 5. (a) The silk gland of the experimental silkworm under (left) white and (right) UV light, respectively. (b) TEM and inset HRTEM images of the ethanol extract from (a). (c) The UV−vis absorption spectra of the ethanol solutions extracted from the posterior silk glands, in comparison with that of G-CDs. (d) PL emission spectra of the ethanol solutions extracted from the integral silk glands (excitation wavelength = 450 nm). (e) PL emission spectra of the ethanol solutions extracted from the anterior, the middle, and the posterior silk glands of the experimental silkworm (excitation wavelength = 450 nm). (f) The ethanol extraction for the integral, anterior, middle, and posterior silk glands of silkworms from (left) the control and (right) the experimental groups under UV light, respectively.

fiber. By the end of the fifth instar the silkworms were fasted for 1 day and then sacrificed and dissected. The exposed organs of the experimental and control groups are compared in Figure S11. Under UV light, the silk glands of the experimental group have obvious green luminescence, while the control have almost no luminescence. In general, mulberry silk is composed of sericin (*ca.* 30 wt %) and fibroin (*ca.* 70 wt %).[66,67] Sericin is mainly secreted by the middle silk gland, which is the thickest part of the whole silk gland and usually aggregates pigments. Fibroin is mainly secreted by the posterior silk gland, which is the longest part. Besides, the anterior silk gland is the most slender part, connecting to the spinneret.[43,44,68−70] As shown in Figure 5 a and Figure S11, the whole silk gland from the experimental group is luminous, green in both the anterior and the posterior while yellow in the middle. But in the control group, only the middle silk gland shows weak yellow fluorescence due to some flavonoid pigments. Thus, the bright yellow-green fluorescence in the experimental silk gland may arise from the superposition of the flavonoids and G-CDs.[64,71,72] After 1 day of fasting, there is no undigested mulberry leaf debris in the digestive tract of the experimental group, which manifests the same green fluorescence with G-CDs. In contrast, the control manifests no green fluorescence but weak yellow fluorescence at the posterior digestive tract, probably owing to the accumulation of flavonoids.[72,73] The whole silk gland and the divided three parts, anterior, middle, and posterior from another silk gland, as well as the digestive tract, are extracted by equal amounts of ethanol, respectively, and displayed in Figure S12. TEM and HRTEM images (Figure 5 b) of the ethanol extract from the whole experimental silk gland show that there are plenty of nanoparticles with the same size and 0.21 nm lattice spacing as G-CDs, confirming that the fluorescent substance in the silk gland is indeed G-CDs.

The UV spectra of ethanol extracts of the different parts in silkworm body were measured as well as that of G-CDs (Figure S13). For the whole, anterior, middle silk gland and the digestive tract, the spectral features of the control and the experiment group are similar, while those of the posterior silk glands are unlike. In Figure 5 c, the curve of the experimental group is close to that of G-CDs, indicating that G-CDs are mainly gathered in the posterior silk gland. The fluorescence spectra of the integral silk gland were tested (Figure 5 d); the intensity of the experimental group is much higher than that of the control group; and the emission peak at 535 nm is the same as that of G-CDs (Figure 1 e). The fluorescence spectra of the other four different silkworm parts are compared in Figure S14. All samples from the experimental group have much stronger fluorescence than those of the control at around 535 nm, except those from the digestive tract (Figure S14 e). Although the control digestive tract also has a fluorescence peak, it is located at 550 nm and looks yellow, in accordance with the anatomy picture in Figure S11. Figure 5 f presents photographs of ethanol extracts from the integral and each part of the silk gland under UV irradiation. As expected, the integral silk glands show significant fluorescence contrast, and the fluorescence color of the experimental group is the same as that of G-CDs. Among the extracts of three different silk gland parts, the fluorescence contrast of the anterior silk gland is the smallest; that of the middle is weak; and their color in daylight is deep. The fluorescence of the posterior silk gland extract of the experimental group is the brightest, and its color in daylight is light. These results indicate that the content of G-CDs in the posterior silk gland is much larger than those in both the anterior and middle silk glands. The fluorescence spectra of

https://doi.org/10.1021/acs.nanolett.4c02426
Nano Lett. 2024, 24, 9675−9682

the ethanol extracts from different silk gland parts in the experimental group (Figure 5 e) also confirm this result. Besides, most of the natural pigments that exhibit deep color but weak fluorescence are located in the middle silk gland.

Figure S15 analyzes the ethanol extract of silkworm feces and depicts the entire metabolic process of G-CDs in the silkworm body. In Figure S15 a, the red fluorescence at 672 nm is ascribed to chlorophyll, which is from mulberry leaves undigested by silkworms.[74,75] The PL spectra indicate that the experimental silkworm feces have both chlorophyll and G-CDs, while the control had only chlorophyll fluorescence. Furthermore, nanoparticles with the typical CD lattice spacing of 0.21 nm are observed in the TEM image of the experimental extract (Figure S15 b). Therefore, the whole metabolic process of G-CDs in a silkworm body can be delineated. G-CDs are sprayed on mulberry leaves, dried, and then ingested by silkworms through feeding. G-CDs first enter the digestive tract and subsequently are transferred by hemolymph to the silk gland (mainly in the posterior part) where G-CDs are mixed with fibroin to form fluorescent silk when weaving cocoons. It is clear that G-CDs undergo the ingestion and excretion in silkworm bodies without affecting their health and maintain their optical features during the whole process. These results demonstrate that G-CDs exhibit very high biosafety, chemical stability, and fluorescent efficiency during their long journey inside silkworms.

A new type of green fluorescent carbon dots, G-CDs, was prepared and sprayed on mulberry leaves for feeding silkworms. From eating G-CDs to spinning cocoons, the silkworms exhibited bright green fluorescence in their whole bodies under UV light, which was visible to the human naked eye. The obtained silk fibers had a smooth surface and good toughness. The silk was reeled to thread and sewn into patterns on the cloth, which were beautiful and dazzling under UV light. The presence of G-CDs in the cocoons, silk glands, and silkworm feces was confirmed by various measurements, indicating that G-CDs were transferred in the silkworm bodies safely without any change. Moreover, G-CDs were enriched in the posterior silk gland and introduced into fibroin, which was outstanding compared to many other feed additives. Such G-CDs have promising potential in producing naturally fluorescent silk fibers for practical applications, suggesting that multifunctional natural silk will come true in the near future by designing CDs as feed additives.

■ ASSOCIATED CONTENT

Supporting Information

The Supporting Information is available free of charge at https://pubs.acs.org/doi/10.1021/acs.nanolett.4c02426.

The additional high-resolution TEM images; PL emission spectra; fine XPS spectrum; XRD patterns; Raman spectrum; the photographic recording of the growth process of silkworms; the photos of silkworm moths and eggs under UV lamps; the photos in detail of various organs after anatomy and their ethanol extracts; additional UV and PL spectra of ethanol extract; and schematic diagram of the metabolic pathway of G-CDs in the silkworm body (PDF)

Video of a moving silkworm in the experimental group (MP4)

Video of a cocooning silkworm in the experimental group (MP4)

■ AUTHOR INFORMATION

Corresponding Author

Huan-Ming Xiong − *Department of Chemistry and Shanghai Key Laboratory of Molecular and Catalysis and Innovative Materials, Fudan University, Shanghai 200438, P. R. China;* orcid.org/0000-0002-3118-942X; Email: hmxiong@fudan.edu.cn

Authors

Zhao-Fan Wu − *Department of Chemistry and Shanghai Key Laboratory of Molecular and Catalysis and Innovative Materials, Fudan University, Shanghai 200438, P. R. China;* orcid.org/0009-0002-6524-4519

Bao-Juan Wang − *Department of Chemistry and Shanghai Key Laboratory of Molecular and Catalysis and Innovative Materials, Fudan University, Shanghai 200438, P. R. China*

Jia-Wen Ni − *Department of Chemistry and Shanghai Key Laboratory of Molecular and Catalysis and Innovative Materials, Fudan University, Shanghai 200438, P. R. China*

Zhao-Nan Sun − *Department of Chemistry and Shanghai Key Laboratory of Molecular and Catalysis and Innovative Materials, Fudan University, Shanghai 200438, P. R. China*

Xi-Rong Zhang − *Department of Chemistry and Shanghai Key Laboratory of Molecular and Catalysis and Innovative Materials, Fudan University, Shanghai 200438, P. R. China*

Complete contact information is available at: https://pubs.acs.org/10.1021/acs.nanolett.4c02426

Author Contributions

The manuscript was written through contributions of all authors. H.-M.X. designed experiments and conceived the manuscript. Z.-F.W. performed most of the experiments and manuscript writing. B.-J.W. contributed to anatomy and imaging experiments. J.-W.N. assisted in characterization tests of carbon dots. Z.-N.S. and X.-R.Z. participated in the analysis of the experimental results. H.-M.X. directed the project. All authors have given approval to the final version of the manuscript.

Notes

The authors declare no competing financial interest.

■ ACKNOWLEDGMENTS

This work was financially supported by the National Natural Science Foundation of China (21975048) and the Shanghai Science and Technology Committee (19DZ2270100).

■ REFERENCES

(1) Cao, C.; Lin, Z.; Liu, X.; Jia, Y.; Saiz, E.; Wolf, S. E.; Wagner, H. D.; Jiang, L.; Cheng, Q. Strong Reduced Graphene Oxide Coated Bombyx Mori Silk. *Adv. Funct. Mater.* **2021**, *31* (34), No. 2102923.

(2) Gholipourmalekabadi, M.; Sapru, S.; Samadikuchaksaraei, A.; Reis, R. L.; Kaplan, D. L.; Kundu, S. C. Silk Fibroin for Skin Injury Repair: Where Do Things Stand? *Adv. Drug Delivery Rev.* **2020**, *153*, 28−53.

(3) Sahoo, J. K.; Hasturk, O.; Falcucci, T.; Kaplan, D. L. Silk Chemistry and Biomedical Material Designs. *Nat. Rev. Chem.* **2023**, *7* (5), 302−318.

(4) Holland, C.; Numata, K.; Rnjak-Kovacina, J.; Seib, F. P. The Biomedical Use of Silk: Past, Present, Future. *Adv. Healthc. Mater.* **2019**, *8* (1), No. 1800465.

(5) Farokhi, M.; Mottaghitalab, F.; Samani, S.; Shokrgozar, M. A.; Kundu, S. C.; Reis, R. L.; Fatahi, Y.; Kaplan, D. L. Silk Fibroin/Hydroxyapatite Composites for Bone Tissue Engineering. *Biotechnol. Adv.* **2018**, *36* (1), 68−91.

(6) Song, Y.; Wang, H.; Yue, F.; Lv, Q.; Cai, B.; Dong, N.; Wang, Z.; Wang, L. Silk-Based Biomaterials for Cardiac Tissue Engineering. *Adv. Healthc. Mater.* **2020**, *9* (23), No. 2000735.
(7) Guo, C.; Li, C.; Mu, X.; Kaplan, D. L. Engineering Silk Materials: From Natural Spinning to Artificial Processing. *Appl. Phys. Rev.* **2020**, *7* (1), No. 011313.
(8) Liu, H.; Sun, Z.; Guo, C. Chemical Modification of Silk Proteins: Current Status and Future Prospects. *Adv. Fiber Mater.* **2022**, *4* (4), 705−719.
(9) Tansil, N. C.; Koh, L. D.; Han, M.-Y. Functional Silk: Colored and Luminescent. *Adv. Mater.* **2012**, *24* (11), 1388−1397.
(10) Liu, C.; Bai, H.; He, B.; He, X.; Zhang, J.; Chen, C.; Qiu, Y.; Hu, R.; Zhao, F.; Zhang, Y.; He, W.; Chau, J. H. C.; Chen, S.; Lam, J. W. Y.; Tang, B. Z. Functionalization of Silk by AIEgens through Facile Bioconjugation: Full-Color Fluorescence and Long-Term Bioimaging. *Angew. Chem., Int. Ed.* **2021**, *60* (22), 12424−12430.
(11) Iizuka, T.; Sezutsu, H.; Tatematsu, K.; Kobayashi, I.; Yonemura, N.; Uchino, K.; Nakajima, K.; Kojima, K.; Takabayashi, C.; Machii, H.; Yamada, K.; Kurihara, H.; Asakura, T.; Nakazawa, Y.; Miyawaki, A.; Karasawa, S.; Kobayashi, H.; Yamaguchi, J.; Kuwabara, N.; Nakamura, T.; Yoshii, K.; Tamura, T. Colored Fluorescent Silk Made by Transgenic Silkworms. *Adv. Funct. Mater.* **2013**, *23* (42), 5232−5239.
(12) Wu, Z.-F.; Sun, Z.-N.; Xiong, H.-M. Fluorescent Silk Obtained by Feeding Silkworms with Fluorescent Materials†. *Chin. J. Chem.* **2023**, *41* (16), 2035−2046.
(13) Ramos, N.; Miranda, M. S.; Franco, A. R.; Silva, S. S.; Azevedo, J.; Dias, I. R.; Reis, R. L.; Viegas, C.; Gomes, M. E. Toward Spinning Greener Advanced Silk Fibers by Feeding Silkworms with Nanomaterials. *ACS Sustain. Chem. Eng.* **2020**, *8* (32), 11872−11887.
(14) Wang, Q.; Wang, C.; Zhang, M.; Jian, M.; Zhang, Y. Feeding Single-Walled Carbon Nanotubes or Graphene to Silkworms for Reinforced Silk Fibers. *Nano Lett.* **2016**, *16* (10), 6695−6700.
(15) Lu, H.; Jian, M.; Yin, Z.; Xia, K.; Shi, S.; Zhang, M.; Wang, H.; Liang, X.; Ma, W.; Zhang, X.; Zhang, Y. Silkworm Silk Fibers with Multiple Reinforced Properties Obtained through Feeding Ag Nanowires. *Adv. Fiber Mater.* **2022**, *4* (3), 547−555.
(16) Nisal, A.; Trivedy, K.; Mohammad, H.; Panneri, S.; Sen Gupta, S.; Lele, A.; Manchala, R.; Kumar, N. S.; Gadgil, M.; Khandelwal, H.; More, S.; Laxman, R. S. Uptake of Azo Dyes into Silk Glands for Production of Colored Silk Cocoons Using a Green Feeding Approach. *ACS Sustain. Chem. Eng.* **2014**, *2* (2), 312−317.
(17) Lu, H.; Jian, M.; Gan, L.; Zhang, Y.; Li, S.; Liang, X.; Wang, H.; Zhu, M.; Zhang, Y. Highly Strong and Tough Silk by Feeding Silkworms with Rare Earth Ion-Modified Diets. *Sci. Bull.* **2023**, *68* (23), 2973−2981.
(18) Tansil, N. C.; Li, Y.; Teng, C. P.; Zhang, S.; Win, K. Y.; Chen, X.; Liu, X. Y.; Han, M.-Y. Intrinsically Colored and Luminescent Silk. *Adv. Mater.* **2011**, *23* (12), 1463−1466.
(19) Liang, J.; Zhang, X.; Ji, Y.; Chen, Z.; Norton, M. L.; Wang, Y.; Yan, C.; Zheng, X.; Zhu, Y.; Cheng, G. Feeding Silkworms with HPMC Dispersed MoO2 NPs: An Efficient Strategy to Enhance the Supercapacitance Performance of Carbonized Silk. *Compos. Sci. Technol.* **2021**, *215*, No. 109025.
(20) Zhan, Q.; Fan, S.; Wang, D.; Yao, X.; Shao, H.; Zhang, Y. Super-Strong and Uniform Fluorescent Composite Silk from Trace AIE Nanoparticle Feeding. *Compos. Commun.* **2020**, *21*, No. 100414.
(21) Li, J.; Li, Y.; Lu, S.; Zhang, J.; Zhang, C.; Xiong, L. Dual-Performance Optimized Silks from Ultra-Low Dose Polymer Dots Feeding and Its Absorption, Distribution and Excretion in the Silkworms. *Adv. Fiber Mater.* **2022**, *4* (4), 845−858.
(22) Yang, Z.; Xu, T.; Li, H.; She, M.; Chen, J.; Wang, Z.; Zhang, S.; Li, J. Zero-Dimensional Carbon Nanomaterials for Fluorescent Sensing and Imaging. *Chem. Rev.* **2023**, *123* (18), 11047−11136.
(23) Wang, H.; Ai, L.; Song, H.; Song, Z.; Yong, X.; Qu, S.; Lu, S. Innovations in the Solid-State Fluorescence of Carbon Dots: Strategies, Optical Manipulations, and Applications. *Adv. Funct. Mater.* **2023**, *33* (41), No. 2303756.
(24) Liu, H.; Zhong, X.; Pan, Q.; Zhang, Y.; Deng, W.; Zou, G.; Hou, H.; Ji, X. A Review of Carbon Dots in Synthesis Strategy. *Coord. Chem. Rev.* **2024**, *498*, No. 215468.
(25) Niu, X.; Zheng, W.; Song, T.; Huang, Z.; Yang, C.; Zhang, L.; Li, W.; Xiong, H. Pyrolysis of Single Carbon Sources in SBA-15: A Recyclable Solid Phase Synthesis to Obtain Uniform Carbon Dots with Tunable luminescenc. *Chin. Chem. Lett.* **2023**, *34* (2), No. 107560.
(26) Xue, S.; Li, P.; Sun, L.; An, L.; Qu, D.; Wang, X.; Sun, Z. The Formation Process and Mechanism of Carbon Dots Prepared from Aromatic Compounds as Precursors: A Review. *Small* **2023**, *19* (31), No. 2206180.
(27) Oladzadabbasabadi, N.; Dheyab, M. A.; Nafchi, A. M.; Ghasemlou, M.; Ivanova, E. P.; Adhikari, B. Turning Food Waste into Value-Added Carbon Dots for Sustainable Food Packaging Application: A Review. *Adv. Colloid Interface Sci.* **2023**, *321*, 103020.
(28) Bian, Z.; Wallum, A.; Mehmood, A.; Gomez, E.; Wang, Z.; Pandit, S.; Nie, S.; Link, S.; Levine, B. G.; Gruebele, M. Properties of Carbon Dots versus Small Molecules from "Bottom-up" Synthesis. *ACS Nano* **2023**, *17* (22), 22788−22799.
(29) Wu, Z.; Liang, Z.; Guo, S.; Xiao, Y.; Sun, Y.; Qu, L.; Li, Z. Resolving Variable Cell Viability-Induced False Negative: Accurate and High-Contrast Fluorescence Diagnosis of Cancer Enabled by Dual Organelle Targeting and Multiple Microenvironmental Parameters Responsive Versatile Carbon Dots. *Sens. Actuators B Chem.* **2022**, *359*, No. 131577.
(30) Algar, W. R.; Massey, M.; Rees, K.; Higgins, R.; Krause, K. D.; Darwish, G. H.; Peveler, W. J.; Xiao, Z.; Tsai, H.-Y.; Gupta, R.; Lix, K.; Tran, M. V.; Kim, H. Photoluminescent Nanoparticles for Chemical and Biological Analysis and Imaging. *Chem. Rev.* **2021**, *121* (15), 9243−9358.
(31) Zhao, B.; Ma, H.; Zheng, M.; Xu, K.; Zou, C.; Qu, S.; Tan, Z. Narrow-Bandwidth Emissive Carbon Dots: A Rising Star in the Fluorescent Material Family. *Carbon Energy* **2022**, *4* (1), 88−114.
(32) Liu, Y.; Wang, B.; Zhang, Y.; Guo, J.; Wu, X.; Ouyang, D.; Chen, S.; Chen, Y.; Wang, S.; Xing, G.; Tang, Z.; Qu, S. Perylenedioic Acid-Derived Carbon Dots with Near 100% Quantum Yield in Aqueous Solution for Lasing and Lighting. *Adv. Funct. Mater.* **2024**, 2401353.
(33) Sun, W.; Zhang, Y.; Yin, G.; Lu, S. Afterglow of Dual-Confined Carbon Dots Ranging from Blue to Near-Infrared. *Adv. Funct. Mater.* **2024**, 2402346.
(34) Ding, H.; Xu, J.; Jiang, L.; Dong, C.; Meng, Q.; Rehman, S. ur; Wang, J.; Ge, Z.; Osipov, V. Yu.; Bi, H. Fluorine-Defects Induced Solid-State Red Emission of Carbon Dots with an Excellent Thermosensitivit. *Chin. Chem. Lett.* **2021**, *32* (11), 3646−3651.
(35) Han, T.; Wang, Y.; Ma, S.; Li, M.; Zhu, N.; Tao, S.; Xu, J.; Sun, B.; Jia, Y.; Zhang, Y.; Zhu, S.; Yang, B. Near-Infrared Carbonized Polymer Dots for NIR-II Bioimaging. *Adv. Sci.* **2022**, *9* (30), No. 2203474.
(36) Wang, Y.; Li, X.; Zhao, S.; Wang, B.; Song, X.; Xiao, J.; Lan, M. Synthesis Strategies, Luminescence Mechanisms, and Biomedical Applications of near-Infrared Fluorescent Carbon Dots. *Coord. Chem. Rev.* **2022**, *470*, No. 214703.
(37) Song, T.-B.; Huang, Z.-H.; Zhang, X.-R.; Ni, J.-W.; Xiong, H.-M. Nitrogen-Doped and Sulfonated Carbon Dots as a Multifunctional Additive to Realize Highly Reversible Aqueous Zinc-Ion Batteries. *Small* **2023**, *19* (31), No. 2205558.
(38) Ma, Y.; Wu, L.; Ren, X.; Zhang, Y.; Lu, S. Toward Kilogram-Scale Preparation of Full-Color Carbon Dots by Simply Stirring at Room Temperature in Air. *Adv. Funct. Mater.* **2023**, *33* (50), No. 2305867.
(39) Niu, X.; Song, T.; Xiong, H. Large Scale Synthesis of Red Emissive Carbon Dots Powder by Solid State Reaction for Fingerprint Identificatio. *Chin. Chem. Lett.* **2021**, *32* (6), 1953−1956.
(40) Zhao, B.; Ma, H.; Jia, H.; Zheng, M.; Xu, K.; Yu, R.; Qu, S.; Tan, Z. Triphenylamine-Derived Solid-State Emissive Carbon Dots for Multicolor High-Efficiency Electroluminescent Light-Emitting Diodes. *Angew. Chem., Int. Ed.* **2023**, *62* (22), No. e202301651.
(41) Fan, S.; Zheng, X.; Zhan, Q.; Zhang, H.; Shao, H.; Wang, J.; Cao, C.; Zhu, M.; Wang, D.; Zhang, Y. Super-Strong and Intrinsically Fluorescent Silkworm Silk from Carbon Nanodots Feeding. *Nano-Micro Lett.* **2019**, *11* (1), 75.

https://doi.org/10.1021/acs.nanolett.4c02426
Nano Lett. 2024, 24, 9675−9682

(42) Liu, J.; Kong, T.; Xiong, H.-M. Mulberry-Leaves-Derived Red-Emissive Carbon Dots for Feeding Silkworms to Produce Brightly Fluorescent Silk. *Adv. Mater.* **2022**, *34* (16), No. 2200152.
(43) Hentzen, D.; Chevallier, A.; Garel, J.-P. Differential Usage of Iso-Accepting tRNASer Species in Silk Glands of Bombyx Mori. *Nature* **1981**, *290* (5803), 267−269.
(44) Ma, L.; Xu, H.; Zhu, J.; Ma, S.; Liu, Y.; Jiang, R.-J.; Xia, Q.; Li, S. Ras1CA Overexpression in the Posterior Silk Gland Improves Silk Yield. *Cell Res.* **2011**, *21* (6), 934−943.
(45) Wang, Y.; Liu, Y.; Hao, X.; Zhou, X.; Peng, H.; Shen, Z.; Smalyukh, I. I.; Xie, X.; Yang, B. Supramolecular Liquid Crystal Carbon Dots for Solvent-Free Direct Ink Writing. *Adv. Mater.* **2023**, *35* (40), No. 2303680.
(46) Cai, H.; Wu, X.; Jiang, L.; Yu, F.; Yang, Y.; Li, Y.; Zhang, X.; Liu, J.; Li, Z.; Bi, H. Lysosome-Targeted Carbon Dots with a Light-Controlled Nitric Oxide Releasing Property for Enhanced Photodynamic Therapy. *Chin. Chem. Lett.* **2024**, *35* (4), No. 108946.
(47) Boukhvalov, D. W.; Osipov, V. Yu.; Murzalinov, D.; Serikkanov, A.; Bi, H. A Comprehensive Model of Carbon Nanodots with 0.21 Nm Lattice Fringes Pattern. *Carbon* **2024**, *225*, No. 119101.
(48) Tang, L.; Ai, L.; Song, Z.; Sui, L.; Yu, J.; Yang, X.; Song, H.; Zhang, B.; Hu, Y.; Zhang, Y.; Tian, Y.; Lu, S. Acid-Triggered Aggregation of Carbon Dots Shifted Their Emission to Give Unexpected Deep-Red Lasing. *Adv. Funct. Mater.* **2023**, *33* (34), No. 2303363.
(49) Poole, S. K.; Poole, C. F. Separation Methods for Estimating Octanol−Water Partition Coefficients. *J. Chromatogr. B* **2003**, *797* (1), 3−19.
(50) Enyedy, É. A.; Hollender, D.; Kiss, T. Lipophilicity of Kinetically Labile Metal Complexes through the Example of Antidiabetic Zn(II) and VO(IV) Compounds. *J. Pharm. Biomed. Anal.* **2011**, *54* (5), 1073−1081.
(51) Disdier, Z.; Savoye, S.; Dagnelie, R. V. H. Effect of Solutes Structure and pH on the N-Octanol/Water Partition Coefficient of Ionizable Organic Compounds. *Chemosphere* **2022**, *304*, No. 135155.
(52) Jerga, R.; Brablecová, V.; Talášková, V.; Tomková, H.; Součková, J.; Barták, P.; Skopalová, J. A Novel Device for the Determination of Liposome/Water Partition Coefficients. *Talanta* **2024**, *269*, No. 125434.
(53) Tansil, N. C.; Li, Y.; Koh, L. D.; Peng, T. C.; Win, K. Y.; Liu, X. Y.; Han, M.-Y. The Use of Molecular Fluorescent Markers to Monitor Absorption and Distribution of Xenobiotics in a Silkworm Model. *Biomaterials* **2011**, *32* (36), 9576−9583.
(54) Li, K.; Zhao, J.; Zhang, J.; Ji, J.; Ma, Y.; Liu, X.; Xu, H. Direct in Vivo Functionalizing Silkworm Fibroin via Molecular Recognition. *ACS Biomater. Sci. Eng.* **2015**, *1* (7), 494−503.
(55) Yang, Y.; Zhao, M.; Lai, L. Surface Activity, Micellization, and Application of Nano-Surfactants—Amphiphilic Carbon Dots. *Carbon* **2023**, *202*, 398−413.
(56) Hou, X.; Xu, J.; Zhou, P.; Dai, L.; Zhang, J.; Xiao, X.; Huo, K. A Shining Transmutation of Lignin into Multicolor Carbon Dots via the Dynamic Solvent-Fractionation Engineering. *Chem. Eng. J.* **2023**, *478*, No. 147363.
(57) Xin, X.; Liu, J.; Liu, X.; Xin, Y.; Hou, Y.; Xiang, X.; Deng, Y.; Yang, B.; Yu, W. Melatonin-Derived Carbon Dots with Free Radical Scavenging Property for Effective Periodontitis Treatment via the Nrf2/HO-1 Pathway. *ACS Nano* **2024**, *18* (11), 8307−8324.
(58) Ai, L.; Song, Z.; Nie, M.; Yu, J.; Liu, F.; Song, H.; Zhang, B.; Waterhouse, G. I. N.; Lu, S. Solid-State Fluorescence from Carbon Dots Widely Tunable from Blue to Deep Red through Surface Ligand Modulation. *Angew. Chem., Int. Ed.* **2023**, *62* (12), No. e202217822.
(59) Ding, H.; Zhou, X.-X.; Zhang, Z.-H.; Zhao, Y.-P.; Wei, J.-S.; Xiong, H.-M. Large Scale Synthesis of Full-Color Emissive Carbon Dots from a Single Carbon Source by a Solvent-Free Method. *Nano Res.* **2022**, *15* (4), 3548−3555.
(60) Li, L.; Li, Y.; Ye, Y.; Guo, R.; Wang, A.; Zou, G.; Hou, H.; Ji, X. Kilogram-Scale Synthesis and Functionalization of Carbon Dots for Superior Electrochemical Potassium Storage. *ACS Nano* **2021**, *15* (4), 6872−6885.
(61) Hu, G.; Wang, Y.; Zhang, S.; Ding, H.; Zhou, Z.; Wei, J.; Li, X.; Xiong, H. Rational Synthesis of Silane-Functionalized Carbon Dots with High-Efficiency Full-Color Solid-State Fluorescence for Light Emitting Diodes. *Carbon* **2023**, *203*, 1−10.
(62) Jiang, L.; Cai, H.; Zhou, W.; Li, Z.; Zhang, L.; Bi, H. RNA-Targeting Carbon Dots for Live-Cell Imaging of Granule Dynamics. *Adv. Mater.* **2023**, *35* (21), No. 2210776.
(63) Gong, Q.; Zhang, X.; Li, W.; Guo, X.; Wu, Q.; Yu, C.; Jiao, L.; Xiao, Y.; Hao, E. Long-Wavelength Photoconvertible Dimeric BODIPYs for Super-Resolution Single-Molecule Localization Imaging in Near-Infrared Emission. *J. Am. Chem. Soc.* **2022**, *144* (48), 21992−21999.
(64) Zhu, L.; Zhang, Y.-Q. Identification and Analysis of the Pigment Composition and Sources in the Colored Cocoon of the Silkworm, Bombyx Mori, by HPLC-DAD. *J. Insect Sci.* **2014**, *14*, 31.
(65) Sakudoh, T.; Sezutsu, H.; Nakashima, T.; Kobayashi, I.; Fujimoto, H.; Uchino, K.; Banno, Y.; Iwano, H.; Maekawa, H.; Tamura, T.; Kataoka, H.; Tsuchida, K. Carotenoid Silk Coloration Is Controlled by a Carotenoid-Binding Protein, a Product of the Yellow Blood Gene. *Proc. Natl. Acad. Sci. U. S. A.* **2007**, *104* (21), 8941−8946.
(66) Happey, F.; Hyde, A. J. Composition of Silk. *Nature* **1952**, *169* (4309), 921−921.
(67) Zhang, Y.; Sheng, R.; Chen, J.; Wang, H.; Zhu, Y.; Cao, Z.; Zhao, X.; Wang, Z.; Liu, C.; Chen, Z.; Zhang, P.; Kuang, B.; Zheng, H.; Shen, C.; Yao, Q.; Zhang, W. Silk Fibroin and Sericin Differentially Potentiate the Paracrine and Regenerative Functions of Stem Cells Through Multiomics Analysis. *Adv. Mater.* **2023**, *35* (20), No. 2210517.
(68) Akai, H.; Kobayashi, M. Sites of Fibroin Formation in the Silk Gland in Bombyx Mori. *Nature* **1965**, *206* (4983), 529−529.
(69) Cao, T.-T.; Zhang, Y.-Q. Processing and Characterization of Silk Sericin from Bombyx Mori and Its Application in Biomaterials and Biomedicines. *Mater. Sci. Eng., C* **2016**, *61*, 940−952.
(70) Ayaz, P.; Li, J.; Jin, W.; Ma, M. Fixation of the Color of Naturally Colored Domestic Silk by Cross-Linking the Sericin with Tetrakis (Hydroxymethyl) Phosphonium Sulfate. *Fibers Polym.* **2020**, *21* (3), 548−554.
(71) Lu, Y.; Luo, J.; An, E.; Lu, B.; Wei, Y.; Chen, X.; Lu, K.; Liang, S.; Hu, H.; Han, M.; He, S.; Shen, J.; Guo, D.; Bu, N.; Yang, L.; Xu, W.; Lu, C.; Xiang, Z.; Tong, X.; Dai, F. Deciphering the Genetic Basis of Silkworm Cocoon Colors Provides New Insights into Biological Coloration and Phenotypic Diversification. *Mol. Biol. Evol.* **2023**, *40* (2), No. msad017.
(72) Hirayama, C.; Mase, K.; Iizuka, T.; Takasu, Y.; Okada, E.; Yamamoto, K. Deficiency of a Pyrroline-5-Carboxylate Reductase Produces the Yellowish Green Cocoon 'Ryokuken' of the Silkworm, Bombyx Mori. *Heredity* **2018**, *120* (5), 422−436.
(73) Tamura, Y.; Nakajima, K.-i.; Nagayasu, K.-i.; Takabayashi, C. Flavonoid 5-Glucosides from the Cocoon Shell of the Silkworm, Bombyx Mori. *Phytochemistry* **2002**, *59* (3), 275−278.
(74) Han, J.; Wang, Y.; Ma, J.; Wu, Y.; Hu, Y.; Ni, L.; Li, Y. Simultaneous Aqueous Two-Phase Extraction and Saponification Reaction of Chlorophyll from Silkworm Excrement. *Sep. Purif. Technol.* **2013**, *115*, 51−56.
(75) Liu, J.; Geng, Y.; Li, D.; Yao, H.; Huo, Z.; Li, Y.; Zhang, K.; Zhu, S.; Wei, H.; Xu, W.; Jiang, J.; Yang, B. Deep Red Emissive Carbonized Polymer Dots with Unprecedented Narrow Full Width at Half Maximum. *Adv. Mater.* **2020**, *32* (17), No. 1906641.

https://doi.org/10.1021/acs.nanolett.4c02426
Nano Lett. 2024, 24, 9675−9682